Topological properties of the limited penetrable horizontal visibility graph family

Minggang Wang,[1,2,3] André L. M. Vilela,[3,4] Ruijin Du,[3,5] Longfeng Zhao,[3] Gaogao Dong,[3,5]
Lixin Tian,[1,5,*] and H. Eugene Stanley[3,†]

[1]*School of Mathematical Science, Nanjing Normal University, Nanjing 210042, Jiangsu, China*
[2]*Department of Mathematics, Nanjing Normal University Taizhou College, Taizhou 225300, Jiangsu, China*
[3]*Center for Polymer Studies and Department of Physics, Boston University, Boston, Massachusetts 02215, USA*
[4]*Universidade de Pernambuco, 50100-010, Recife-PE, Brazil*
[5]*Energy Development and Environmental Protection Strategy Research Center, Jiangsu University, Zhenjiang, 212013 Jiangsu, China*

(Received 26 November 2017; revised manuscript received 27 March 2018; published 14 May 2018)

The limited penetrable horizontal visibility graph algorithm was recently introduced to map time series in complex networks. In this work, we extend this algorithm to create a directed-limited penetrable horizontal visibility graph and an image-limited penetrable horizontal visibility graph. We define two algorithms and provide theoretical results on the topological properties of these graphs associated with different types of real-value series. We perform several numerical simulations to check the accuracy of our theoretical results. Finally, we present an application of the directed-limited penetrable horizontal visibility graph to measure real-value time series irreversibility and an application of the image-limited penetrable horizontal visibility graph that discriminates noise from chaos. We also propose a method to measure the systematic risk using the image-limited penetrable horizontal visibility graph, and the empirical results show the effectiveness of our proposed algorithms.

DOI: 10.1103/PhysRevE.97.052117

I. INTRODUCTION

The complex network analysis of univariate or multivariate time series has recently attracted the attention of researchers working in a wide range of fields. Over the past decade several methodologies have been proposed for mapping time series in complex networks [1–9]. These methods include constructing a complex network from a pseudoperiodic time series [2], using a visibility graph algorithm [3], a recurrence network method [4], a stochastic method [5], a coarse geometry theory [6], a nonlinear mutual information method [7], event synchronization [8], and a phase-space coarse-graining method [9]. These methods have been widely used to solve problems in a variety of research fields [10–20].

Among all of these time series analysis algorithms, visibility algorithms are the most efficient when constructing a complex network from a time series. Visibility algorithms are a family of rules for mapping a real-value time series on graphs, which display different cases or scenarios. In all cases each time series datum is assigned to a node, but the connection criterion depend on the algorithm used. For example, in the natural visibility graph (NVG), two nodes i and j are connected if the geometrical criterion $x(t_k) < x(t_i) + [x(t_j) - x(t_i)]\frac{t_k - t_i}{t_j - t_k}, \forall t_k \in (t_i, t_j)$ is fulfilled within the time series [3]. In the parametric natural visibility graph (PNVG) case there are three steps when using this algorithm to map a time series into a complex network: (i) build a natural visibility graph as described above; (ii) set the direction and the angle $\eta_{ij} = \arctan\frac{x(t_j) - x(t_i)}{t_j - t_i}$ with $i < j$ for every link of the natural visibility graph; and (iii) use the parameter view angle rule η, $\eta_{ij} < \eta$ to select links from the directed and weighted graph [21]. In the horizontal visibility graph (HVG) case, the algorithm is similar to the natural visibility graph but it has a modified mapping criterion. In this algorithm, two nodes i and j are connected if $x(t_k) < \inf(x(t_i), x(t_j)), \forall t_k \in (t_i, t_j)$ [22]. These visibility algorithms have been successfully implemented in a variety of fields [23–25].

Recently, a limited penetrable visibility graph (LPVG) [26,27] and a multiscale limited penetrable horizontal visibility graph (MLPHVG) [28] were developed from the visibility graph and the horizontal visibility graph to analyze nonlinear time series. The limited penetrable visibility graph and multiscale limited penetrable horizontal visibility graph have been successfully used to analyze a variety of real signals across different fields, e.g., experimental flow signals and electroencephalogram signals [2,27–30]. Research has shown that the limited penetrable visibility graph and multiscale limited penetrable horizontal visibility graph inherit the merits of the visibility graph, but they are also more resistant to noise, which makes them particularly useful when analyzing signals polluted by unavoidable noise.

There are abundant empirical results that have been obtained using the visibility graph algorithm and its extensions, e.g., the parametric natural visibility graph [21], the horizontal visibility graph [22], the limited penetrable visibility graph [26], and the multiscale limited penetrable horizontal visibility graph [28]. Thus far there has been little research focusing on rigorous theoretical results. Recently Lacasa *et al.* presented topological properties of the horizontal visibility graph associated with random time series [22], periodic series [31], and other stochastic and chaotic processes [32]. They extended the family of visibility algorithms to map scalar fields of an

*tianlx@ujs.edu.cn
†hes@bu.edu

arbitrary dimension onto graphs. They also provided analytical results on the topological properties of the graphs associated with different types of real-value matrices [33]. Wang *et al.* [34] focused on a class of general horizontal visibility algorithms, the limited penetrable horizontal visibility graph (LPHVG), and presented exact results on the topological properties of this visibility graph associated with random series. Here we use previous works [2,31–34] and focus our attention on the limited penetrable horizontal visibility graph, where we present some of its analytical properties.

This paper is organized as follows. In Sec. II we introduce the limited penetrable horizontal visibility graph family. In Sec. III we derive the analytical properties of the different versions of associated limited penetrable horizontal visibility graph for a generic random time series (or a random matrix). We also present several numerical simulations used to check their accuracy. In Sec. IV we show some applications of the directed-limited penetrable horizontal visibility graph and of the image-limited penetrable horizontal visibility graph. In Sec. V we present our conclusions.

II. LIMITED PENETRABLE HORIZONTAL VISIBILITY GRAPH FAMILY

The LPHVG algorithm [28,34] and its extensions are called the LPHVG family. We here present three versions of the LPHVG algorithm with limited penetrable distance ρ, the limited penetrable horizontal visibility graph, LPHVG(ρ), the directed-limited penetrable horizontal visibility graph, DLPHVG(ρ), and the image-limited penetrable horizontal visibility graph of order n, ILPHVG$_n(\rho)$.

A. Limited Pepnetrable horizontal visibility graph

The limited penetrable horizontal visibility graph [LPHVG(ρ)] [34] is a geometrically simpler and analytically solvable version of the visibility graph [3], the limited penetrable visibility graph [26], and the multiscale limited penetrable horizontal visibility graph [28]. To define it, we let $X_N(t)$ be a time series of N real numbers $x_1,x_2,x_3,\ldots,x_N$. We set the limited penetrable distance to ρ, and LPHVG(ρ) maps the time series into a graph with N nodes and adjacency matrix $\mathbf{A}$. Nodes x_i and x_j are connected through an undirected edge ($A_{ij} = A_{ji} = 1$) if x_i and x_j have a limited penetrable horizontal visibility (see Fig. 1), i.e., if $\rho \geqslant 0$ intermediate data x_q follows

$$x_q \geqslant \inf\{x_i,x_j\}, \quad \forall q \in (i,j), \quad \aleph(q) \leqslant \rho, \tag{1}$$

where $\aleph(q)$ is the number of q. The graph spanned by this mapping is the limited penetrable horizontal visibility graph [LPHVG(ρ)]. When we set the limited penetrable distance ρ to 0, then LPHVG(0) degenerates into an horizontal visibility graph [22]. When $\rho \neq 0$ there are more connections between any two LPHVG(ρ) nodes than in horizontal visibility graph. Figure 1(b) shows the newly established connections (dashed red lines) when we infer the LPHVG(1) using horizontal visibility graph. Note that the LPHVG(ρ) of a time series has all the properties of its corresponding horizontal visibility graph, e.g., it is connected and invariant under affine transformations of series data [22].

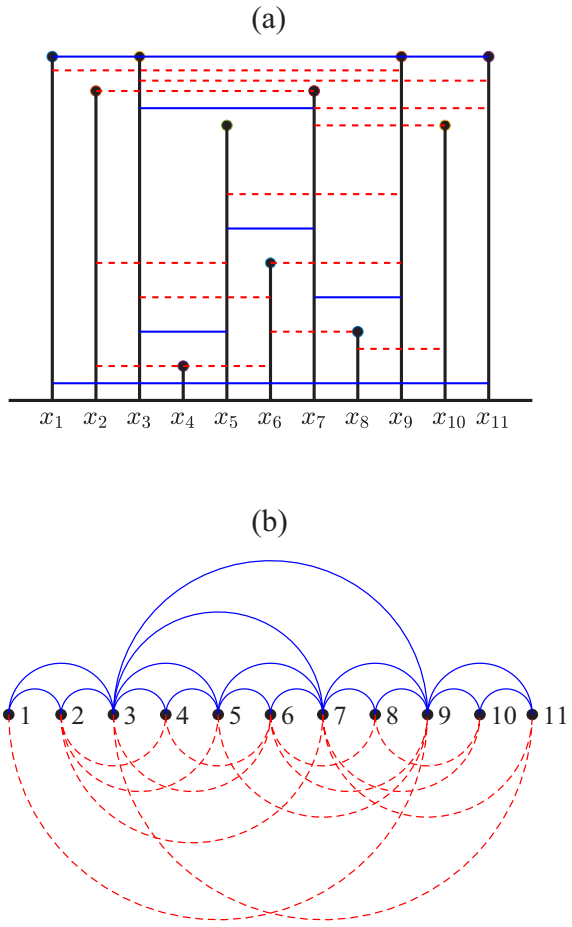

FIG. 1. Example of (a) a time series with 11 data values and (b) its corresponding LPHVG(1), where every node corresponds to time series data in the same order. The horizontal penetrable visibility lines between data points define the links connecting nodes in the graph.

B. Directed limited penetrable horizontal visibility graph

The limited penetrable horizontal visibility graph [LPHVG(ρ)] is undirected, because penetrable visibility does not have a predefined temporal arrow. Directionality can be added by using directed networks. Here we address the directed version and define a directed-limited penetrable horizontal visibility graph [DLPHVG(ρ)], where the degree $k(x_t)$ of the node x_t is split between an ingoing degree $k_{\text{in}}(x_t)$ and an outgoing degree $k_{\text{out}}(x_t)$ such that $k(x_t) = k_{\text{in}}(x_t) + k_{\text{out}}(x_t)$. We define the ingoing degree $k_{\text{in}}(x_t)$ to be the number of links of node x_t with past nodes associated with data in the series, i.e., nodes with $t' < t$. Conversely, we define the outgoing degree $k_{\text{out}}(x_t)$ to be the number of links with future nodes, i.e., nodes with $t'' > t$. Thus DLPHVG(ρ) maps the time series into a graph with N nodes and an adjacency matrix $\mathbf{A} = \mathbf{A}_{\text{in}} + \mathbf{A}_{\text{out}}$, where $\mathbf{A}_{\text{in}}$ is a lower triangular matrix and $\mathbf{A}_{\text{out}}$ is a upper triangular matrix. Nodes $x_{t'}$ and x_t, $t' < t$ (or x_t and $x_{t''}$, $t < t''$) are connected through a directed edge $x_{t'} \to x_t$, i.e., $A_{t't} = 1$ (or $x_t \to x_{t''}$, i.e., $A_{tt''} = 1$) if it satisfies Eq. (1). Figure 2 shows a graphical representation of this algorithm.

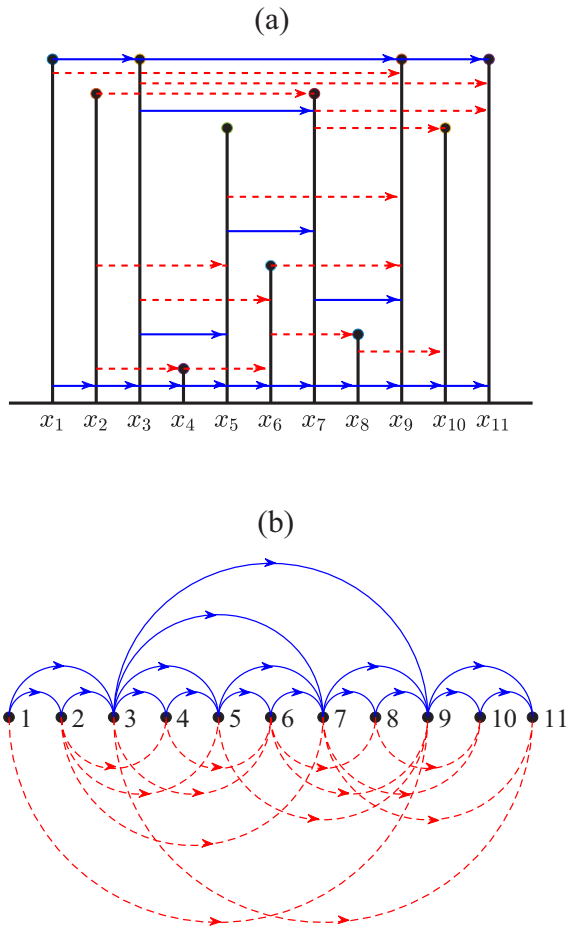

FIG. 2. Graphical illustration of DLPHVG(1). (a) Plot of a sample time series $X_N(t)$ for $N = 11$. Each datum in the series is mapped to a node in the graph. Arrows link the nodes and describe allowed directed penetrable visibility. (b) Plot of the associated DLPHVG(1). In this graph, each node has an ingoing degree k_{in}, which accounts for the number of links with past nodes, and an outgoing degree k_{out}, which in turn accounts for the number of links with future nodes.

For the degree distribution $P(k)$, we use the ingoing and outgoing degree distributions of a DLPHVG(ρ) to define the probability distributions of k_{out} and k_{in} on the graph, which are $P_{\text{out}}(k) \equiv P(k_{\text{out}} = k)$ and $P_{\text{in}}(k) \equiv P(k_{\text{in}} = k)$, respectively. We observe an asymmetry of the resulting graph in a first approximation when we use the invariance of the outgoing (or ingoing) degree series under a time reversal.

C. Image-limited penetrable horizontal visibility graph of order *n*

One-dimensional versions of the limited penetrable horizontal visibility graph [LPHVG(ρ)] and directed-limited penetrable horizontal visibility graph [DLPHVG(ρ)] are used to map landscapes (time series) on complex networks. As in the definition of image visibility graph of order n (IVG$_n$) [33], the definition of LPHVG(ρ) can also be extended and applied to two-dimensional manifolds by extending the LPHVG(ρ) criteria of Eq. (1) along one-dimensional sections of the manifold. To define the image-limited penetrable horizontal

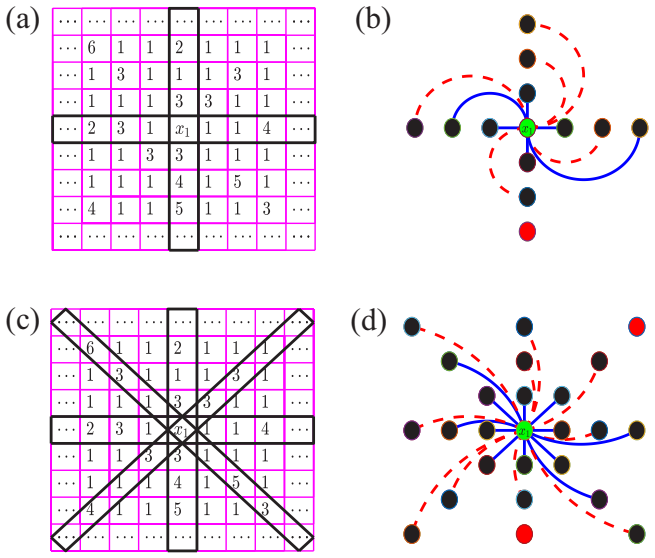

FIG. 3. Graphical illustration of ILPHVG$_n(\rho)$ for $x_1 = 2$. In Fig. 3(a) we depict a sample matrix when x_1 is the central entry, which shows the ILPHVG$_4(1)$ algorithm is evaluated along the vertical and horizontal directions. In Fig. 3(b) illustrates the connectivity pattern associated to x_1 in the case of ILPHVG$_4(1)$. Fig. 3(c) shows the ILPHVG$_8(1)$ algorithm evaluated both along the vertical and horizontal directions and along diagonal directions. In Fig. 3(d) we show the connectivity pattern associated to x_1.

visibility graph of order n [ILPHVG$_n(\rho)$] we let $\mathbf{X}$ be a $N \times N$ matrix for an arbitrary entry (i,j) and partition the plane into n directions such that direction p is at an angle with the row axis of $2\pi(p-1)/n$, where $p = 1,2,\ldots,n$. The image-limited penetrable visibility graph of order n, ILPHVG$_n(\rho)$, has N^2 nodes, each of which is labeled using a pair (i,j) associated with the entry indices x_{ij}, such that two nodes, x_{ij} and $x_{i'j'}$, are linked when (i) $x_{i'j'}$ belongs to one of the n angular partition lines, and (ii) x_{ij} and $x_{i'j'}$ are linked in the LPHVG(ρ) defined over the ordered sequence that includes (i,j) and (i',j'). For example, in ILPHVG$_4(1)$ the penetrable visibility between two points x_{ij} and $x_{i'j'}$ is

$$i = i', \quad x_{iq} \geqslant \inf\{x_{ij}, x_{i'j'}\}, \quad \forall q \in (j,j'), \quad \aleph(q) \leqslant \rho, \quad (2)$$

or

$$j = j', \quad x_{qj} \geqslant \inf\{x_{ij}, x_{i'j'}\}, \quad \forall q \in (i,i'), \quad \aleph(q) \leqslant \rho. \quad (3)$$

Figure 3(a) shows a sample matrix in which x_1 is the central entry, which shows the ILPHVG$_4(1)$ algorithm evaluated along the vertical and horizontal directions. Figure 3(b) shows the connectivity pattern associated to the entry x_1 of the ILPHVG$_4(1)$ algorithm. Figure 3(c) shows the ILPHVG$_8(1)$ algorithm evaluated along the vertical, horizontal, and diagonal directions. Figure 3(d) shows the connectivity pattern associated to the entry x_1 of the ILPHVG$_8(1)$ algorithm.

III. THEORETICAL RESULTS ON THE TOPOLOGICAL PROPERTIES

Theorem 1. [34] If we let $X(t)$ be a bi-infinite sequence of independent and identically distributed (i.i.d.) random variable

x with probability density $f(x)$, then the degree distribution of its associated LPHVG(ρ) is

$$P(k) = \begin{cases} \frac{1}{2\rho+3}\left(\frac{2\rho+2}{2\rho+3}\right)^{k-2(\rho+1)}, & k \geqslant 2\rho+2, \\ 0, \quad \text{otherwise.} \end{cases}$$

The mean degree $\langle k \rangle$ is

$$\langle k \rangle = 4(\rho+1).$$

Reference [34] provides a lengthy proof of this theorem. We here propose an alternative shorter proof.

Proof. We let x be an arbitrary datum of the i.i.d. random time series where its limited penetrable horizontal visibility is interrupted by two bounding data, one datum x_{bl} on its left and one x_{br} on its right. There are 2ρ penetrable data that are larger than x between the two bounding data, ρ penetrable data $x_{\text{pl}}^1, x_{\text{pl}}^2, \ldots, x_{\text{pl}}^\rho$ on the left and ρ data $x_{\text{pr}}^1, x_{\text{pr}}^2, \ldots, x_{\text{pr}}^\rho$ on the right of x. These $2\rho+2$ data are independent of $f(x)$, then

$$\begin{aligned} \Phi_{2\rho+2} = & \int_{-\infty}^{\infty}\int_{x}^{\infty}\int_{x}^{\infty}\int_{x}^{\infty}\ldots\int_{x}^{\infty}\int_{x}^{\infty}\ldots\int_{x}^{\infty} f(x)f(x_{\text{bl}}) \\ & \times f(x_{\text{br}})f\left(x_{\text{pl}}^1\right)\ldots f\left(x_{\text{pl}}^\rho\right)f\left(x_{\text{pr}}^1\right)\ldots f\left(x_{\text{pr}}^\rho\right)dx_{\text{pr}}^\rho \\ & \ldots dx_{pr}^1 dx_{\text{pl}}^\rho \ldots \ldots dx_{\text{pl}}^1 dx_{\text{br}} dx_{\text{bl}} dx. \end{aligned} \tag{4}$$

We define the cumulative probability distribution function $F(x)$ of any probability distribution $f(x)$ as

$$F(x) = \int_{-\infty}^{x} f(t)dt. \tag{5}$$

Then, we rewrite Eq. (4)

$$\Phi_{2\rho+2} = \int_{-\infty}^{\infty} f(x)[1-F(x)]^{2\rho+2}dx = \frac{1}{2\rho+3}. \tag{6}$$

The probability $P(k)$ that the datum penetrates no more than ρ time seeing k data is

$$P(k) = \Phi(k)\Phi_{2\rho+2} = \frac{1}{2\rho+3}\Phi(k), \tag{7}$$

where $\Phi(k)$ is the probability that datum x penetrates no more than ρ time, seeing at least k data. We can recurrently calculate $\Phi(k)$

$$\begin{aligned} & \Phi(k) = \Phi(k-1)(1-\Phi_{2\rho+2}) = \frac{2\rho+2}{2\rho+3}\Phi(k-1), \\ & \Phi(2\rho+2) = 1, \end{aligned} \tag{8}$$

from which we deduce

$$\Phi(k) = \left(\frac{2\rho+2}{2\rho+3}\right)^{k-2(\rho+1)} \Phi(2\rho+2) = \left(\frac{2\rho+2}{2\rho+3}\right)^{k-2(\rho+1)}. \tag{9}$$

Thus, we finally obtain

$$P(k) = \begin{cases} \Phi(k)\Phi_{2\rho+2} = \frac{1}{2\rho+3}\left(\frac{2\rho+2}{2\rho+3}\right)^{k-2(\rho+1)}, & k \geqslant 2\rho+2, \\ 0, \quad \text{otherwise.} \end{cases} \tag{10}$$

Then the mean degree $\langle k \rangle$ of the limited penetrable horizontal visibility graph associated to an uncorrelated random process is

$$\begin{aligned} \langle k \rangle &= \sum_{k=2\rho+2}^{\infty} kP(k) = \sum_{k=2\rho+2}^{\infty} \frac{k}{2\rho+3}\left(\frac{2\rho+2}{2\rho+3}\right)^{k-2(\rho+1)} \\ &= 4(\rho+1). \end{aligned} \tag{11}$$

Theorem 1 shows the exact degree distribution for LPHVG(ρ), which indicates that the degree distribution $P(k)$ of LPHVG(ρ) associated to i.i.d. random time series has a unified exponential form, independent of the probability distribution from which the series was generated.

Theorem 2. We let $X(t)$ be a bi-infinite sequence of i.i.d. random variable x with probability density $f(x)$, and consider a limited penetrable horizontal visibility graph associated with $X(t)$. We let $\langle k(x) \rangle$ be a mean degree of the node associated with a datum of height x and define it as

$$\begin{aligned} & \langle k(x) \rangle \\ & = 2(\rho+1) - 2(\rho+1)ln[1-F(x)], F(x) = \int_{-\infty}^{x} f(t)dt. \end{aligned}$$

Proof. We define $P(k|x)$ to be the conditional probability that a given node has degree k when its height is x. Using the constructive proof process of $P(k)$ in Ref. [34], we calculate $P(k|x)$

$$\begin{aligned} & P(k|x) \\ & = \sum_{h=0}^{k-\theta}(2\rho+1)^h \frac{(-1)^{k-\theta}}{h!(k-\theta-h)!}[1-F(x)]^\theta \{ln[1-F(x)]\}^{k-\theta} \\ & = [1-F(x)]^\theta \{\theta ln[1-F(x)]\}^{k-\theta}\frac{(-1)^{k-\theta}}{(k-\theta)!}, \theta = 2(\rho+1). \end{aligned} \tag{12}$$

Then $\langle k(x) \rangle$ is

$$\langle k(x) \rangle = \sum_{k=2(\rho+1)}^{\infty} kP(k|x). \tag{13}$$

We let $k-2(\rho+1) = \alpha$, $2(\rho+1)ln[1-F(x)] = \lambda$ and deduce

$$\begin{aligned} \langle k(x) \rangle &= 2(\rho+1)[1-F(x)]^{2(\rho+1)} \sum_{\alpha=0}^{\infty} \frac{(-1)^\alpha \lambda^\alpha}{\alpha!} \\ &\quad + [1-F(x)]^{2(\rho+1)} \sum_{\alpha=1}^{\infty} \frac{(-1)^\alpha \lambda^\alpha}{(\alpha-1)!} \\ &= 2(\rho+1) - \lambda = 2(\rho+1) - 2(\rho+1)ln[1-F(x)]. \end{aligned} \tag{14}$$

Theorem 2 shows the relation between data height x and the mean degree of the nodes associated with the data of height x. The result indicates that the $\langle k(x) \rangle$ is a monotonically increasing function of x and we conclude that the hubs of LPHVG(ρ) are the data with largest values. We checked the accuracy of the result within finite series and Fig. 4(a) shows a plot of the numerical values of $\langle k(x) \rangle$ of LPHVG(ρ), with $\rho = 0,2,4$, and 6 associated to a random series of 1000 data extracted from a uniform distribution for $F(x) = x$. The theoretical results (red lines) show a good agreement with the data [Eq. (14)].

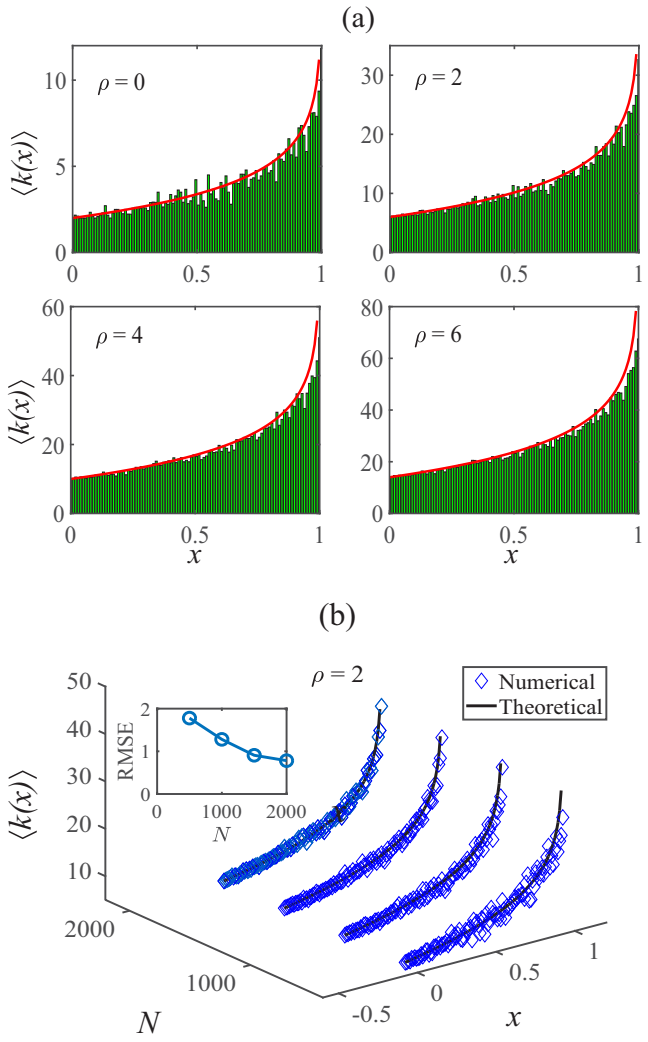

FIG. 4. (a) The relation between data height x and the node degree $\langle k(x)\rangle$ under different penetrable distance ρ. (b) The relation between data height x and the node degree $\langle k(x)\rangle$ under different time series size N.

To investigate the finite size effect, Fig. 4(b) shows a plot of the numerical values of $\langle k(x)\rangle$ of LPHVG(2) associated with random series of 500, 1000, 1500, 2000 data. We use root mean square error (RMSE) to measure the agreement between the numerical and theoretical results. We find that when the size N of the time series increases, the RMSE between the numerical and theoretical results decreases, improving its accuracy.

Theorem 3. We let $X(t)$ be an infinite periodic series of period T with no repeated values within a period. The normalized mean distance $\langle\rangle$ of LPHVG(ρ) associated with $X(t)$ is

$$\langle d\rangle \sim [4(\rho+1) - \langle k(T)\rangle],$$

where

$$\langle k(T)\rangle = 4(\rho+1)\left(1 - \frac{2\rho+1}{2T}\right), \quad \rho \ll T.$$

Proof. To calculate $\langle k(T)\rangle$ we consider an infinite periodic series of period T with no repeated values in a period and denote it $X(t) = \{...,x_0,x_1,x_2,...,x_T,x_1,x_2,...\}$, $x_0 = x_T$. We let $\rho \ll T$ for the subseries $\tilde{X}(t) = \{x_0,x_1,x_2,...,x_T\}$ and, without loss of generality, we assume that $x_0 = x_T$ corresponds to the largest value of the subseries $\tilde{X}(t)$, and $x_1,...,x_\rho,x_{T-\rho},...x_{T-1}$ corresponds to the 2nd to $(2\rho+1)$nd largest value of the subseries. Thus, we construct the LPHVG(ρ) associated with subseries $\tilde{X}(t)$. We assume that LPHVG(ρ) has E links and let x_i be the smallest datum of the subseries $\tilde{X}(t)$. Because no data repetitions are allowed in $\tilde{X}(t)$, the degree of x_i is $2(\rho+1)$ when the graph is constructed from LPHVG(ρ). We now remove node x_i and its $2(\rho+1)$ links from LPHVG(ρ). The resulting graph now has $E - 2(\rho+1)$ links and T nodes. We iterate this operation $T - (2\rho+1)$ times and the resulting graph has $2(\rho+1)$ nodes, i.e., $x_0,x_1,...,x_\rho,x_{T-\rho},...x_{T-1},x_T$. When these $2(\rho+1)$ nodes are connected by $E_r = \binom{2\rho+2}{2}$ links, the total number of deleted links are $E_d = 2(\rho+1)[T-(2\rho+1)]$. Thus, the mean degree of a limited penetrable horizontal visibility graph associated with $X(t)$ is

$$\begin{aligned}\langle k(T)\rangle &= 2\frac{E_d + E_r}{T} \\ &= \frac{2\{2(\rho+1)[T-(2\rho+1)] + (\rho+1)(2\rho+1)\}}{T} \\ &= 4(\rho+1)\left(1 - \frac{2\rho+1}{2T}\right), \quad \rho \ll T. \end{aligned} \tag{15}$$

We let $\langle\ell\rangle$ be the mean distance of LPHVG(ρ), N be the number of nodes, and the normalized mean distance be $\langle d\rangle = \frac{\langle\ell\rangle}{N}$. Note that $\langle d\rangle$ depends on T for horizontal visibility graph associated with periodic orbits $\langle d\rangle \sim T^{-1}$ for $N \to \infty$ [31]. Thus, we deduce that $\langle d\rangle \sim T^{-1}$ for LPHVG(ρ). Using Eq. (15), we obtain $T^{-1} \sim [4(\rho+1) - \langle k(T)\rangle]$ and

$$\langle d\rangle \sim [4(\rho+1) - \langle k(T)\rangle]. \tag{16}$$

This result holds for every periodic or aperiodic series ($T \to \infty$), independent of the deterministic process that generates them, because the only constraint in its derivation is that data within a period can not be repeated. Note that one consequence of Eq. (15) is that each time series has an associated LPHVG(ρ) with a maximum mean degree (for a aperiodic series) of $\langle k(\infty)\rangle = 4(\rho+1)$, which agrees with the previous result in Eq. (11). In Eq. (16) the limiting solution $\langle k(T)\rangle \to 4(\rho+1), \langle d\rangle \to 0$ holds for all aperiodic, chaotic, and random series. To check the accuracy of the analytical result, we generate four periodic time series ($T = 50$, 100, 200, and 250) with 2000 data points. The data in each period come from a Logistic map with $\mu = 4$ [34]. We construct the limited penetrable horizontal visibility graphs with penetrable distance $\rho = 0,1,2,...,10$ associated with this periodic time series. Figure 5(a) shows a plot of the mean degree of the resulting LPHVG(ρ) values with different ρ values that indicate a good agreement with the theoretical results in Eq. (15). Figure 5(b) shows a calculation of the normalized mean distance $\langle d\rangle$ of LPHVG(ρ) values with $\rho = 0$, 1, and 2 associated with the period time series of $T = 100,200,300,...,1000$. The numerical values of the mean normalized distance $\langle d\rangle$ as a function of mean degree $\langle k(T)\rangle$ agrees with the theoretical linear relation of Eq. (16).

Theorem 4. [34] We let $X(t)$ be a real value bi-infinite time series of i.i.d. random variables x with probability

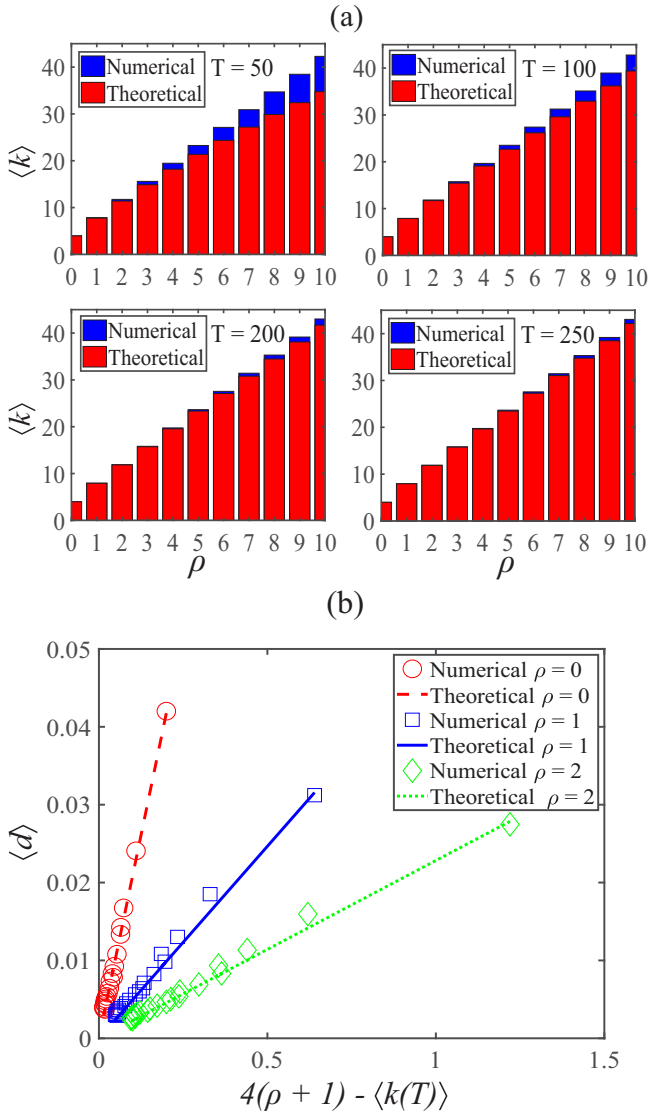

FIG. 5. (a) Numerical results of Eq. (15) where we simulated a periodic time series for $T = 50,100,200$, and 250, respectively, with 2000 data points. (b) Numerical results of Eq. (16), where we simulated a periodic time series with $T = 100,200,300,...,1000$. The data in each period comes from the Logistic map with $\mu = 4$.

distribution $f(x)$ and examine its associated LPHVG(ρ). The local clustering coefficient distribution is then

$$P(C_{\min}) = \frac{1}{2\rho+3}\exp\left\{\left[\frac{\varphi+\sqrt{\varphi^2-8C_{\min}(2\rho+1)}}{2C_{\min}}-2(\rho+1)\right]\times\ln\left(\frac{2\rho+2}{2\rho+3}\right)\right\},$$

and

$$P(C_{\max}) = \frac{1}{2\rho+3}\exp\left\{\left[\frac{\phi+\sqrt{\phi^2-8C_{\max}(6\rho+1)}}{2C_{\max}}-2(\rho+1)\right]\times\ln\left(\frac{2\rho+2}{2\rho+3}\right)\right\},$$

where $\varphi = C_{\min} + 2(\rho+1)$ and $\phi = C_{\max} + 2(2\rho+1)$.

Theorem 5. [34] We let $X_N(t)$ be a bi-finite sequence of i.i.d. random variables extracted from a continuous probability density $f(x)$. Then the probability $P_\rho(n)$ that two data separated by n intermediate data are two connected nodes in the LPHVG(ρ) is

$$P_\rho(n) = \frac{2\rho(\rho+1)+2}{n(n+1)}, \quad \rho = 0,1,2,...$$

Theorem 4 shows the distribution characteristics of the minimum and the maximum clustering coefficients of the nodes in LPHVG(ρ). Theorem 5 indicates that the limited penetrable visibility probability $P_\rho(n) = \frac{2\rho(\rho+1)+2}{n(n+1)}$ introduces shortcuts in the LPHVG(ρ). With these shortcuts the limited penetrable horizontal visibility graph reveals the presence of small-world phenomena [34].

Theorem 6. We let $X(t)$ be a bi-infinite sequence of i.i.d. of random variable x with a probability density $f(x)$. Then both the in and out degree distribution of its associated DLPHVG(ρ) is

$$P_{\text{in}}(k) = P_{\text{out}}(k) = \begin{cases} \frac{1}{\rho+2}\left(\frac{\rho+1}{\rho+2}\right)^{k-(\rho+1)}, & k \geqslant \rho+1, \\ 0, & \text{otherwise.} \end{cases}$$

Proof. Let x be an arbitrary datum of the i.i.d. random time series with $x \leqslant x_{\text{br}}$, and $P_{\text{out}}(k)$ be the probability that its limited penetrable horizontal visibility is interrupted by one bounding datum on its right. There are ρ penetrable data $x_{p1},x_{p2},...,x_{p\rho} \geqslant x$ between x and the bounding data x_{br}. These $\rho+1$ data are independent of $f(x)$. Then

$$\Phi_{\text{out}}^{\rho+1} = \int_{-\infty}^{\infty}\int_{x}^{\infty}...\int_{x}^{\infty}\int_{x}^{\infty} f(x)f(x_{p1})...f(x_{p\rho})f(x_{\text{br}}) \times dx_{\text{br}}dx_{p\rho}...dx_{p1}dx = \int_{-\infty}^{\infty} f(x)[1-F(x)]^{\rho+1}dx = \frac{1}{\rho+2}. \quad (17)$$

The probability $P_{\text{out}}(k)$ that datum x penetrates no more than ρ times, seeing k data is

$$P_{\text{out}}(k) = \Phi_{\text{out}}(k)\Phi_{\text{out}}^{\rho+1} = \frac{1}{\rho+2}\Phi_{\text{out}}(k), \quad (18)$$

where $\Phi(k)$ is the probability that x penetrates no more than ρ times to the right, seeing at least k data. Then $\Phi(k)$ can be recurrently calculated

$$\Phi(k) = \Phi(k-1)\left(1-\Phi_{\text{out}}^{\rho+1}\right) = \frac{\rho+1}{\rho+2}\Phi(k-1) = \left(\frac{\rho+1}{\rho+2}\right)^{k-(\rho+1)}\Phi(\rho+1), \quad (19)$$

from which, with $\Phi(\rho+1) = 1$, we deduce

$$\Phi(k) = \left(\frac{\rho+1}{\rho+2}\right)^{k-(\rho+1)}. \quad (20)$$

Thus, we finally obtain

$$P_{\text{out}}(k) = \Phi_{\text{out}}(k)\Phi_{\text{out}}^{\rho+1} = \begin{cases} \frac{1}{\rho+2}\left(\frac{\rho+1}{\rho+2}\right)^{k-(\rho+1)}, \\ 0, \quad \text{otherwise.} \end{cases} \quad (21)$$

To further check the accuracy of Eq. (21), we perform several numerical simulations. We generate random series

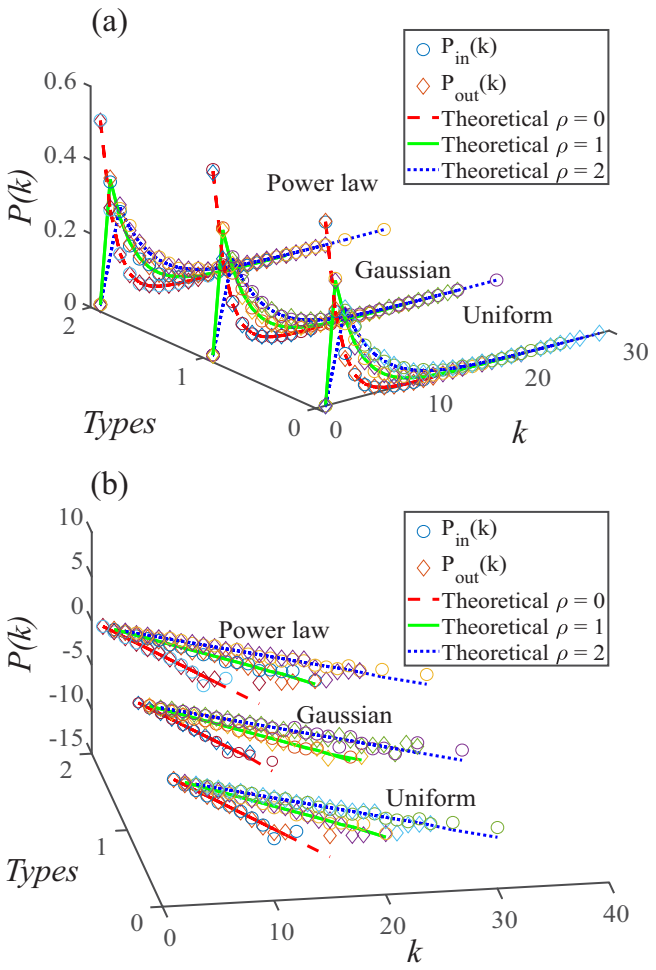

FIG. 6. (a) Plot of the in and out degree distributions of the resulting graphs. (b) Semilog plot of the in and out degree distributions of the resulting graphs. The theoretical results showed were calculated using Eq. (21).

of 3000 data points from uniform, gaussian, and power law distributions and their associated DLPHVG(ρ). Figure 6 shows plots of the degree distributions with penetrable distances $\rho = 0$, 1 and 2. We find that the theoretical results agree with the numerics, placing aside finite size effects. As in the degree distribution of LPHVG(ρ) [34], the deviations between the tails of the in and out degree distributions of DLPHVG(ρ) associated with i.i.d. random series are caused solely by finite size effects.

Theorem 7. We let $\mathbf{X}$ be a $N \times N$ matrix with entries $x_{ij} = \xi$, where ξ is a random variable sampled from a distribution $f(x)$. Then when $n > 0$ and in the limit $N \to \infty$, the degree distribution of the associated ILPHVG$_n(\rho)$ converges to

$$P(k) = \begin{cases} \frac{1}{[n(\rho+1)+1]}\left[\frac{n(\rho+1)}{n(\rho+1)+1}\right]^{k-n(\rho+1)}, & k \geqslant n(\rho+1). \\ 0, \text{ otherwise.} \end{cases}$$

Proof. To derive general results, we consider the two special cases $n = 4$ and $n = 8$. In the case $n = 4$, we let x be an arbitrary datum in $\mathbf{X}$, where the probability of its image-limited penetrable horizontal visibility is interrupted by four bounding datum, i.e., $x_{\rm br}$ on its right, $x_{\rm ba}$ above it, $x_{\rm bl}$ on its left, and $x_{\rm bb}$ below it. There are 4ρ penetrable data $x_{\rm pr1},\ldots,x_{{\rm pr}\rho},x_{\rm pa1},\ldots,x_{{\rm pa}\rho},x_{\rm pl1},\ldots,x_{{\rm pl}\rho},x_{\rm pb1}\ldots,x_{{\rm pb}\rho}$ between x and the four bounding data. These $4\rho + 4$ data are independent of $f(x)$. Then

$$\begin{aligned}
&\Phi[4(\rho+1)] \\
&= \int_{-\infty}^{\infty}\int_{x}^{\infty}\ldots\int_{x}^{\infty}\int_{x}^{\infty}\ldots\int_{x}^{\infty}\int_{x}^{\infty}\ldots\int_{x}^{\infty}\int_{x}^{\infty}\ldots \\
&\quad \ldots\int_{x}^{\infty}\int_{x}^{\infty}\int_{x}^{\infty}\int_{x}^{\infty}\int_{x}^{\infty} f(x)f(x_{\rm pr1})\ldots f(x_{{\rm pr}\rho})f(x_{\rm pa1})\ldots \\
&\quad \ldots f(x_{{\rm pa}\rho})f(x_{\rm pl1})\ldots f(x_{{\rm pl}\rho})f(x_{\rm pb1})\ldots f(x_{{\rm pb}\rho})f(x_{\rm br})f(x_{\rm ba}) \\
&\quad \times f(x_{\rm bl})f(x_{\rm bb})dx_{\rm bb}dx_{\rm bl}dx_{\rm ba}dx_{\rm br}dx_{{\rm pb}\rho}\ldots dx_{\rm pb1}dx_{{\rm pl}\rho}\ldots \\
&\quad \ldots dx_{\rm pl1}dx_{{\rm pa}\rho}\ldots dx_{\rm pa1}dx_{{\rm pr}\rho}\ldots dx_{\rm pr1}dx \\
&= \int_{-\infty}^{\infty} f(x)[1-F(x)]^{4\rho+4}dx = \frac{1}{4\rho+5}. \qquad (22)
\end{aligned}$$

The probability that the node x has a penetrable visibility of exactly k nodes is

$$\begin{aligned}
P(k) &= \{1-\Phi[4(\rho+1)]\}^{k-4(\rho+1)}\Phi[4(\rho+1)] \\
&= \frac{1}{4\rho+5}\left(\frac{4\rho+4}{4\rho+5}\right)^{k-4(\rho+1)}, \quad k \geqslant 4(\rho+1). \qquad (23)
\end{aligned}$$

Similarly, when $n = 8$ from Eq. (22), then

$$\Phi[8(\rho+1)] = \int_{-\infty}^{\infty} f(x)[1-F(x)]^{8\rho+8}dx = \frac{1}{8\rho+9}. \qquad (24)$$

Here the probability that node x has a penetrable visibility of exactly k nodes is

$$\begin{aligned}
P(k) &= \{1-\Phi[8(\rho+1)]\}^{k-8(\rho+1)}\Phi[8(\rho+1)] \\
&= \frac{1}{8\rho+9}\left(\frac{8\rho+8}{8\rho+9}\right)^{k-8(\rho+1)}, \quad k \geqslant 8(\rho+1). \qquad (25)
\end{aligned}$$

From Eqs. (23) and (25) we deduce for a generic n

$$\begin{aligned}
P(k) &= \{1-\Phi[n(\rho+1)]\}^{k-n(\rho+1)}\Phi[n(\rho+1)] \\
&= \begin{cases} \frac{1}{[n(\rho+1)+1]}\left[\frac{n(\rho+1)}{n(\rho+1)+1}\right]^{k-n(\rho+1)}, & k \geqslant n(\rho+1). \\ 0, \quad \text{otherwise.} \end{cases} \qquad (26)
\end{aligned}$$

Note that when $n = 2$ this result reduces to that in Eq. (10). To check the accuracy of Eq. (26), we estimate the degree distribution of ILPHVG$_n(\rho)$ associated with $N \times N$ random matrices whose entries are i.i.d. uniform random variables between 0 and 1. To illustrate the finite size effects, we also define the cutoff value k_0. When $k > k_0$, all the degree distributions of the numerical results are smaller than the theoretical result in Eq. (26). Figures 7(a)–7(c) and 7(e)–7(g) show semilog plots of the finite-size degree distributions of ILPHVG$_4(\rho)$ and ILPHVG$_8(\rho)$ with $N = 200$. Note that the distributions agree with Eq. (26) when $k \leqslant k_0$. To assess the convergence speed of Eq. (26) for finite N, we estimate the cutoff value k_0 for different finite N sizes [see Figs. 7(d) and 7(h)]. Note that the location of the cutoff value k_0 scales logarithmically with the system size N, i.e., finite size effects only affect the tail of the distribution, which quickly converges with N.

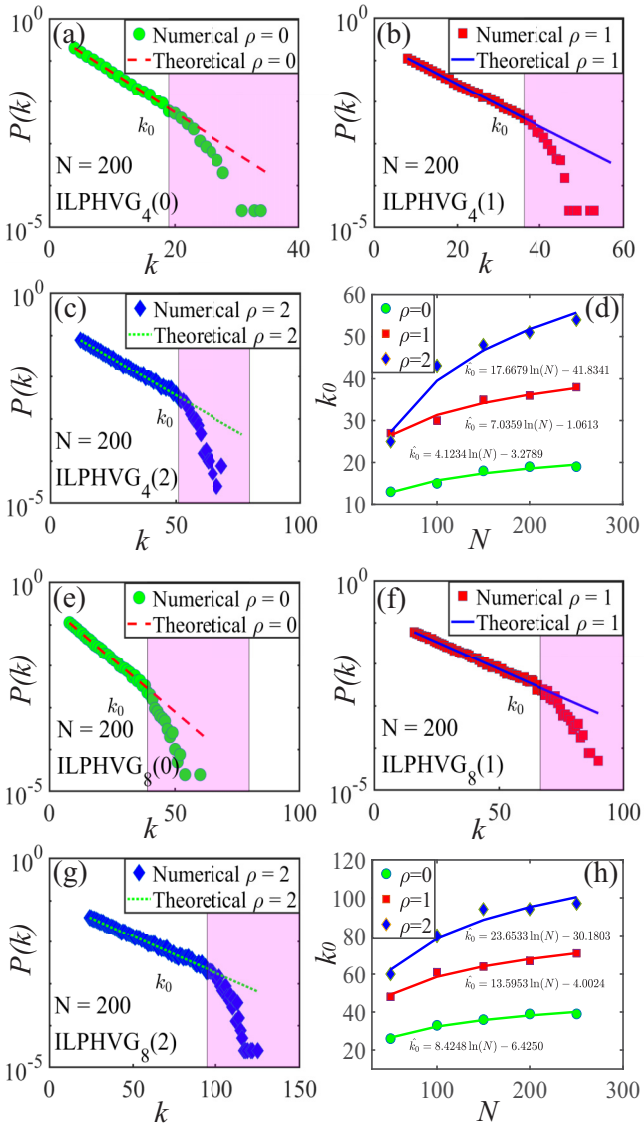

FIG. 7. (a) Semilog plot of the degree distribution of ILPHVG$_4(\rho)$ associated to $N \times N$ random matrices. The solid line is the theoretical value of $P(k)$ given by Eq. (26). In every case we find an good agreement with this equation for $k \leqslant k_0$, where k_0 is a cutoff value that denotes the onset of finite size effects. (b) Plot of the cutoff k_0 as a function of different size N for $n = 4$, suggesting a logarithmic scaling. (c) Semilog plot of the degree distribution of ILPHVG$_8(\rho)$ associated to $N \times N$ random matrices and the theoretical value of $P(k)$. (d) Plot of the cutoff k_0 as a function of different size N for $n = 8$, also suggesting a logarithmic scaling.

In addition to the above proof method for degree distributions of LPHVG(ρ) (Theorem 1), DLPHVG(ρ) (Theorem 6), and ILPHVG$_n(\rho)$ (Theorem 7), we can also prove them from the construction process of LPHVG(ρ), DLPHVG(ρ), and ILPHVG$_n(\rho)$. We here give the proof for ILPHVG$_n(\rho)$, and the proofs for LPHVG(ρ) and DLPHVG(ρ) follow analogously. Generating a panel data of size $N \times N$ is equivalent to putting $N \times N$ numbers into $N \times N$ positions. In the first step, we randomly choose a position and put the largest number on it. In the second step, we choose a position from the remaining $N^2 - 1$ positions and put the second largest number on it.

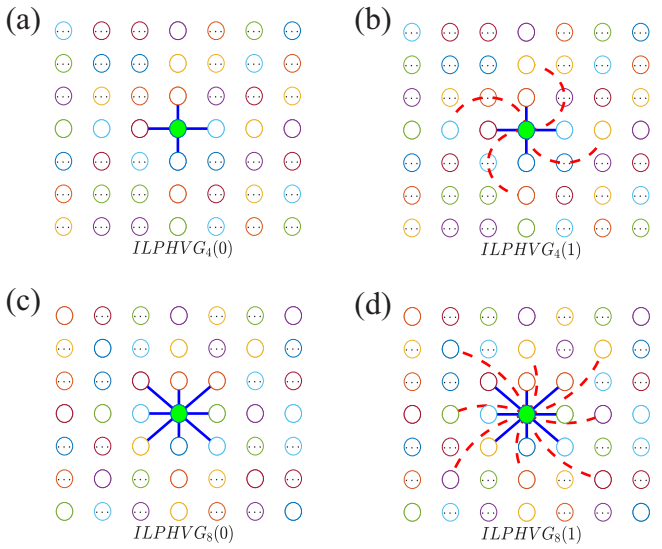

FIG. 8. Graphical illustration of the new edges generated of ILPHVG$_4(\rho)$ and ILPHVG$_8(\rho)$ with $\rho = 0$ and 1 when we add the l^2th largest number (the green node) into ILPHVG$_4(\rho)$ and ILPHVG$_8(\rho)$.

In step l, we randomly choose a position from $N^2 - l + 1$ remaining positions and put the largest number l on it.

To derive the general results of a ILPHVG$_n(\rho)$ using iterative construction process, we first examine the two special cases $n = 4$ and $n = 8$. When $n = 4$, we construct the ILPHVG$_n(\rho)$ from a matrix with $l^2 - 1$ numbers in step l^2. We define $L_I(k,l^2 - 1)$ the number of nodes with degree k. When we add largest number l^2 into the ILPHVG$_4(\rho)$, only $4(\rho + 1)$ new edges are generated, as shown in Fig. 8(a) with $\rho = 0$, in Fig. 8(b) with $\rho = 2$, where the green node is the largest number l^2 node and the $4(\rho + 1)$ new edges link to the $4(\rho + 1)$ nodes adjacent to node l^2. The degree of each $4(\rho + 1)$ node increases by 1. Because the new node is placed randomly, $l^2 - 1$ nodes have the same probability $4(\rho + 1)/(l^2 - 1)$ of changing their degrees. With a probability $1 - 4(\rho + 1)/(l^2 - 1)$ the other nodes degrees remain the same. So the number of nodes with degree k in the new ILPHVG$_4(\rho)$ containing l^2 nodes is

$$L_4(k,l^2) = \left[1 - \frac{4(\rho+1)}{l^2-1}\right] L_4(k,l^2-1) + \frac{4(\rho+1)}{l^2-1} L_4(k-1,l^2-1) + \delta_{k,4(\rho+1)}, \quad (27)$$

where

$$\delta_{k,4(\rho+1)} = \begin{cases} 1, & k = 4\rho + 4, \\ 0, & \text{otherwise}, \end{cases}$$

because the degree of each new node is $k = 4(\rho + 1)$. The probability that nodes with degree k in the ILHVG$_4(\rho)$ containing l^2 nodes is calculated by

$$P_4(k,l^2) = L_4(k,l^2)/l^2. \quad (28)$$

Thus, we rewrite Eq. (28) to be

$$P_4(k,l^2) \approx \left(1 - \frac{4\rho+5}{l^2}\right) P_4(k,l^2-1) + \frac{4(\rho+1)}{l^2} P_4(k-1,l^2-1), \quad (29)$$

in which $\delta_{k,2(\rho+1)}/l^2 = 0$ for large l^2. When $l^2 \to \infty$, we have

$$P_4(k-1,l^2) = P_4(k-1,l^2-1) = P_4(k-1),$$
$$P_4(k,l^2) = P_4(k,l^2-1) = P_4(k). \quad (30)$$

Combining Eqs. (29) and (30), we obtain

$$P_4(k) = \frac{4\rho+4}{4\rho+5}P_4(k-1). \quad (31)$$

By applying $\sum_{k=4(\rho+1)}^{\infty} P_4(k) = 1$, we obtain the solution to Eq. (31),

$$P_4(k) = \frac{(4\rho+5)^{4\rho+3}}{(4\rho+4)^{4\rho+4}}\left(\frac{4\rho+4}{4\rho+5}\right)^k. \quad (32)$$

Similarly, when $n = 8$ we add the largest number l^2 into the ILPHVG$_8(\rho)$, and $8(\rho+1)$ new edges are generated shown in Fig. 8(c) with $\rho = 0$, Fig. 8(d) with $\rho = 2$, the green node is the largest number l^2 node, and $8(\rho+1)$ new edges link to $8(\rho+1)$ nodes adjacent to node l^2. We then change Eq. (27) to

$$L_8(k,l^2) = \left[1 - \frac{8(\rho+1)}{l^2-1}\right]L_8(k,l^2-1) + \frac{8(\rho+1)}{l^2-1}L_8(k-1,l^2-1) + \delta_{k,8(\rho+1)}. \quad (33)$$

Thus,

$$P_8(k,l^2) \approx \left(1 - \frac{8\rho+9}{l^2}\right)P_8(k,l^2-1) + \frac{8(\rho+1)}{l^2}P_8(k-1,l^2-1). \quad (34)$$

When $l^2 \to \infty$, we have

$$P_8(k) = \frac{8\rho+8}{8\rho+9}P_8(k-1). \quad (35)$$

By applying $\sum_{k=8(\rho+1)}^{\infty} P_{I8}(k) = 1$ we obtain the solution to Eq. (35)

$$P_8(k) = \frac{(8\rho+9)^{8\rho+7}}{(8\rho+8)^{8\rho+8}}\left(\frac{8\rho+8}{8\rho+9}\right)^k. \quad (36)$$

From Eqs. (32) and (36), we deduce the probability for a generic n,

$$P_n(k) = \frac{[n(\rho+1)+1]^{n(\rho+1)-1}}{[n(\rho+1)]^{n(\rho+1)}}\left[\frac{n(\rho+1)}{n(\rho+1)+1}\right]^k. \quad (37)$$

This result is consistent with the analytical expression Eq. (26).

IV. APPLICATION OF DLPHVG(ρ) AND ILPHVG$_n(\rho)$

We use the analytical results of LPHVG(ρ) to describe the global evolution of crude oil futures and to distinguish between random and chaotic signals [34]. We also discuss some applications of DLPHVG(ρ) and ILPHVG$_n(\rho)$.

TABLE I. Values of the irreversibility measure associated to the degree distribution $D_{\mathrm{KL}}[P_{\mathrm{out}}(k)||P_{\mathrm{in}}(k)]$ for DLPHVG(ρ) associated to series of 3000 data generated from reversible and irreversible processes.

Series description	$\rho = 0$	$\rho = 1$	$\rho = 2$
Uniform distribution	0.000950	0.007106	0.007269
Gaussian distribution	0.002633	0.007106	0.005507
Power law distribution	0.000226	0.004257	0.005267
Logistic map ($\mu = 4$)	0.342985	0.090773	0.081985
Hénon map ($a = 1.4, b = 0.3$)	0.158358	0.125637	0.140270

A. Measure real-valued time series irreversibility by DLPHVG(ρ)

Time series irreversibility is an important topic in basic and applied science [35]. Over the past decade several methods of measuring time irreversibility have been proposed [36–38]. A recent proposal uses the directed horizontal visibility algorithm [39]. Here the Kullback-Leibler divergence between the out- and in-degree distributions is defined by

$$D_{\mathrm{KL}}[P_{\mathrm{out}}(k)||P_{\mathrm{in}}(k)] = \sum_k P_{\mathrm{out}}(k)\log\frac{P_{\mathrm{out}}(k)}{P_{\mathrm{in}}(k)}. \quad (38)$$

Equation (38) measures the irreversibility of real-value stationary stochastic series, and here we explore the applicability of DLPHVG(ρ). We first select an appropriate parameter ρ, then we map a time series to a directed-limited penetrable horizontal visibility graph, and we use Eq. (38) to estimate the degree of irreversibility of the series. Using Theorem 6 and Eq. (38) we find that the Kullback-Leibler divergence between the in and out degree distributions associated with an i.i.d. random infinite series is equal to zero. Using finite size analysis, we find that this quantity tends asymptotically to zero for finite series of size N. We set $\rho = 0$, 1, and 2, and calculate the numerical value of the Kullback-Leibler divergence of the random series of 3000 data from uniform, Gaussian, and power-law distributions (see the upper section of Table I). All numerical values for D_{KL} are approximately 0, which suggests that the i.i.d. time series is reversible.

We next examine the chaotic Logistic ($\mu = 4$) and Hénon ($a = 1.4, b = 0.3$) map series. Figures 9(a) and 9(b) show plots of the in and out degree distributions of DLPHVG(ρ), $\rho = 0, 1$, and 2 associated with the Logistic map at $\mu = 4$ and the Hénon map for $a = 1.4$ and $b = 0.3$ of 3000 data points. Note that in each case there is a clear distinction between the in and out degree distributions, and this differs from the i.i.d. series case [see Fig. 6(b)]. We calculate the values of the Kullback-Leibler divergence for each case (bottom section of Table I) and we find that these values are positive and much larger than those of the i.i.d. series. Figures 9(c) and 9(d) show a finite size analysis for chaotic maps. Note that the D_{KL} values associated with the chaos maps converges asymptotically to a nonzero value for a series of size N, which indicates that chaos maps are irreversible. Thus by selecting an appropriate parameter for ρ, the $D_{\mathrm{KL}}[P_{\mathrm{out}}(k)||P_{\mathrm{in}}(k)]$ of DLPHVG(ρ) captures the irreversibility of the time series.

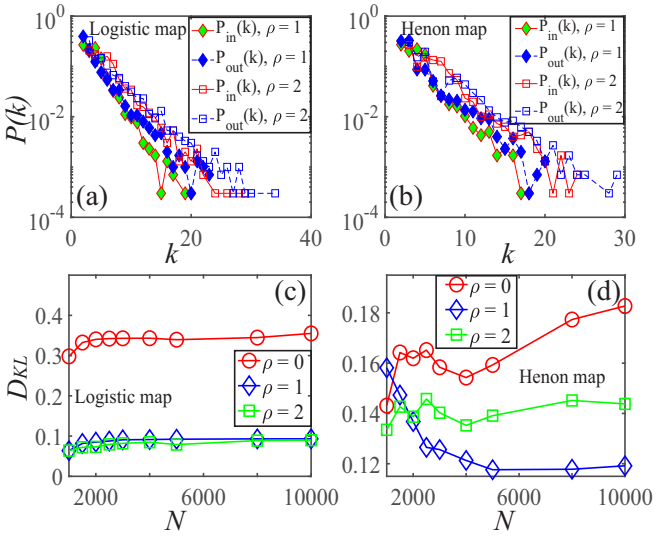

FIG. 9. Plot of the in and out degree distributions of DLPHVG(ρ), $\rho = 0,1$, and 2 associated to (a) the chaotic Logistic map at ($\mu = 4$) of 3000 data points and to the (b) Hénon map for ($a = 1.4, b = 0.3$) of 3000 data points, which different from the uncorrelated cases. Values of the Kullback-Leibler divergence D_{KL} associated to (c) the logistic map with series size N and (d) the Hénon map with series size N, which converge asymptotically to a nonzero value.

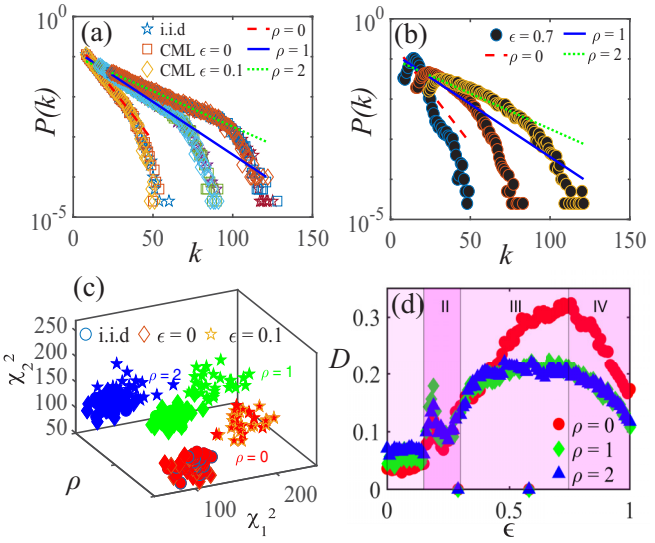

FIG. 10. (a) Semilog plot of the degree distribution of ILPHVG$_8(\rho)$, $\rho = 0,1$, and 2 associated to a two-dimensional uncorrelated random field of uniform random variables (stars), and two-dimensional coupled map lattices of diffusively coupled fully chaotic logistic maps, for coupling constant $\epsilon = 0$ (squares) and $\epsilon = 0.1$ (diamonds). The dashed red, solid blue, and dotted green lines are the results of Eq. (26) for $\rho = 0$, $\rho = 1$, and $\rho = 2$, respectively. (b) Semilog plot of the degree distribution of ILPHVG$_8(\rho)$, $\rho = 0,1$, and 2 associated to two-dimensional coupled map lattices of diffusively coupled fully chaotic logistic maps, for coupling constant $\epsilon = 0.7$ (black dots). (c) The χ^2 statistic in two-dimensional phase space (time delay $\tau = 2$). (d) Scalar parameter D as a function of the coupling constant ϵ, computed from the degree distribution of ILPHVG$_8(\rho)$, $\rho = 0,1$, and 2 associated to 100×100 CMLs of chaotic logistic maps.

B. Discriminating between noise and chaos using ILPHVG$_n(\rho)$

Although chaotic processes display an irregular and unpredictable behavior that is frequently perceived to be random, chaos is a deterministic process that often hides patterns that can be extracted using appropriate techniques. In recent decades, some research efforts to distinguish between noise and chaos have been widespread, and applications have been developed in all scientific disciplines involving complex, irregular empirical signals [40–42]. Lacasa*et al.* [33] used visibility graphs to distinguish spatiotemporal chaos from simple randomness. We also examine spatially extended structures and explore whether ILPHVG$_n(\rho)$ can distinguish spatiotemporal chaos from simple randomness.

We define $\mathbf{X}(t)$ to be a two-dimensional square lattice of N^2 diffusively-coupled chaotic maps that evolve in time [33]. In each vertex of this coupled map lattice (CML) we allocate a fully chaotic logistic map $x_{t+1} = Q(x_t)$, with $Q(x) = 4x(1 - x)$, and the system is then spatially coupled,

$$x_{ij}(t+1) = (1-\epsilon)Q[x_{ij}(t)] + \frac{\epsilon}{4}\sum_{i',j'} Q[x_{i'j'}(t)], \qquad (39)$$

where the sum extends to the Von Neumann neighborhood of ij (four adjacent neighbors). We use periodic boundary conditions with coupling strength $\epsilon \in [0,1]$. Figure 10(a) shows a semilog plot for $N = 200$ of the degree distribution of ILPHVG$_8(\rho)$, $\rho = 0,1$, and 2 associated with a two-dimensional uncorrelated random field of uniform random variables (stars), and a two-dimensional coupled map lattice of diffusively coupled fully chaotic logistic maps for $\epsilon = 0$ (squares) and $\epsilon = 0.1$ (diamonds). Figure 10(b) shows a plot of the degree distribution of ILPHVG$_8(\rho)$, $\rho = 0,1$, and 2 associated with the two-dimensional coupled map lattices of diffusively coupled chaotic logistic maps for $\epsilon = 0.7$. Equation (26) shows $\rho = 0$ (dashed red line), $\rho = 1$ (solid blue line), and $\rho = 2$ (dotted green line).

Figures 10(a) and 10(b) show that the degree distribution of ILPHVG$_8(\rho)$, $\rho = 0,1$, and 2 associated with the uncoupled ($\epsilon = 0$) and weakly coupled ($\epsilon = 0.1$) cases is indistinguishable from the degree distribution associated with the i.i.d. random field. Figure 10(b) shows that the degree distribution deviates from the theoretical result in Eq. (26) only in the strongly coupled case ($\epsilon = 0.7$). Note that the coupled map lattices from Eq. (39) when $\epsilon > 0$ the degree distributions of ILPHVG$_8(\rho)$ are statistically different from the theoretical result in Eq. (26). Nevertheless, the degree distribution of ILPHVG$_8(\rho)$, $\rho = 0,1$, and 2, associated with the i.i.d. random field, uncoupled case ($\epsilon = 0$), and weakly coupled case ($\epsilon = 0.1$) are well approximated by Eq. (26). There are deviations for $k > k_0$ ($k_0 = 19$ for $\rho = 0$, $k_0 = 36$ for $\rho = 1$, and $k_0 = 51$ for $\rho = 2$), but they are caused by finite-size effects (see Fig. 7). To quantify potential deviations of the uncoupled and weakly coupled cases from Eq. (26), we compute χ^2 that measures the deviation between the empirical degree distribution and the theoretical result

$$\chi^2 = N^2 \sum_k \frac{[P_{\mathrm{num}}(k) - P_{\mathrm{theo}}(k)]^2}{P_{\mathrm{theo}}(k)}, \qquad (40)$$

where $P_{\text{num}}(k)$ is the degree distribution of the numerical result and $P_{\text{theo}}(k)$ is the theoretical result from Eq. (26). Here we consider 30 realizations of the i.i.d. random field and for the uncoupled ($\epsilon = 0$) and the weakly coupled map lattices ($\epsilon = 0.1$), we use $8 \leqslant k \leqslant 44$ for $\rho = 0$, $16 \leqslant k \leqslant 77$ for $\rho = 1$, and $24 \leqslant k \leqslant 99$ for $\rho = 2$ to compute the χ^2 statistic. Figure 10(c) shows the calculated results in a two-dimensional phase space with a time delay $\tau = 2$. Note that there are clear distinctions between the uncorrelated i.i.d. random field, the uncoupled map lattices ($\epsilon = 0$), and the weakly coupled map lattices ($\epsilon = 0.1$) for $\rho = 0$ and $\rho = 1$, but when $\rho = 2$ the distinction is no longer clear. We thus select an appropriate parameter ρ and use the degree distribution of ILPHVG(ρ) to distinguish noise from chaos.

Note that when we increase the coupling constant ϵ the spatiotemporal dynamics of the coupled map lattice shows a rich phase diagram. Using the degree distribution of ILPHVG$_8(\rho)$, we show this spatiotemporal dynamic process. For each ϵ we compute the degree distribution of the associated ILPHVG$_8(\rho)$ and then we compute the distance D between the degree distribution at ϵ and the corresponding result for $\epsilon = 0$ in Eq. (26),

$$D = \sum_k \left| P_\rho(k) - \frac{1}{8\rho+9}\left(\frac{8\rho+8}{8\rho+9}\right)^{k-8(\rho+1)} \right|, \tag{41}$$

where $P_\rho(k)$ is the degree distribution of ILPHVG$_n(\rho)$, and D is a scalar order parameter that describes the spatial configuration of the CML. Figure 10(d) shows that when $\rho = 0, 1$, and 2, the evolution of D with ϵ changes from 0 to 1, indicating sharp changes in the different phases—fully developed turbulence with weak spatial correlations (I), periodic structure (II), spatially coherent structure (III), and mixed structure (IV)—between periodic and spatially coherent structures [33]. Thus, the degree distribution of the ILPHVG$_8(\rho)$ can capture the special spatial structure.

C. Measure the systematic risk using ILPHVG$_n(\rho)$

Estimation of systematic risk has always been a hot issue in research of system science [43–50]. Over the past decade several methods of measuring systematic risk have been proposed, such as the absorption ratio [44], the β coefficient[45], the network methods [47–49], multivariate autoregressive conditional heteroscedasticity method [50]. Here, we propose a method to measure the systematic risk using ILPHVG$_n(\rho)$. There are four steps in the proposed method, i.e., construct sliding window, map the panel data into ILPHVG$_n(\rho)s$, calculate the correlation index matrix, and calculate the risk index.

Step 1. Construct sliding window. To characterize the evolution process of the panel data $\mathbf{X}_{N\times T} = \{x_{ij}\}$, $i = 1,2,...,N$ and $j = 1,2,...,T$ using ILPHVG$_n(\rho)$, we divide the entire scale of the panel data into equal small-scale segments (or windows) and assume that the length of the sliding window is L. From the definition of ILPHVG$_n(\rho)$, we let $L = N$. We define l as the step length between sliding time windows and to ensure that small-scale segments of the time series are continuous, we require that $l < L$. This allows us to obtain $T' = [(T - L)/l + 1]$ for small-scale time windows, where [...] denotes the rounding function.

Step 2. Map the panel data into ILPHVG$_n(\rho)$s. In this step, we first need to determine the value of parameter ρ and we compute the absolute distance function $\Delta(\rho)$,

$$\Delta(\rho) = \left|\chi^2_{\text{Real}} - \chi^2_{\text{Rand}}\right|, \tag{42}$$

where χ^2_{Real} and χ^2_{Rand} are χ^2 values for real and random panel data, respectively. The larger Δ means a better distinction between the real panel data and the random panel data. Thus, we can determine the value of parameter ρ using Eq. (42). In general, we set $n = 4$ or $n = 8$ and then, for every small-scale time window t, we transform the panel data into the a ILPHVG$_n(\rho)$ of time t. The topological structure of ILPHVG$_n(\rho)$ changes with time t, therefore, we write ILPHVG$_n(\rho,t)$, $t = 1,2,...,T'$.

Step 3. Calculate the correlation index matrix. We use the Euclidean distance to measure the relationship between ILPHVG$_n(\rho)$s. We define the Euclidean distance between ILPHVG$_n(\rho,t_m)$ and ILPHVG$_n(\rho,t_n)$ to be

$$d_{t_m,t_n} = \sqrt{\sum_{i=1}^{L}\sum_{j=1}^{L}[a_{ij}(t_m) - a_{ij}(t_n)]}, \tag{43}$$

where $a_{ij}(t_m) \in \mathbf{A}(t_m)$ and $a_{ij}(t_n) \in \mathbf{A}(t_n)$, where $\mathbf{A}$ is the adjacency matrix. We then determine the distance matrix

$$\mathbf{D}_{T'\times T'} = \left\{d_{t_m,t_n}\right\}; \quad t_m = 1,2,...,T'; \quad t_n = 1,2,...,T', \tag{44}$$

and assign a threshold value to ν

$$\nu = \min\left\{d^{\text{rand}}_{t_m,t_n}\right\}_{t_m\neq t_n}, \quad d^{\text{rand}}_{t_m,t_n} \in \mathbf{D}^{\text{rand}}_{T'\times T'}, \tag{45}$$

here $\mathbf{D}^{\text{rand}}_{T'\times T'}$ is the distance matrix associated with i.i.d. random panel data. From Eq. (45), we can see that ν can be obtained from the distance matrix of ILPHVG$_n(\rho)$s associated with the i.i.d. panel data, which is the critical value to measure the correlation between the data in different time periods. Using the threshold ν, we define the correlation index γ,

$$\gamma(t_m,t_n) = \begin{cases} 0, & d_{t_m,t_n} \geqslant \nu, \\ 1 - d_{t_m,t_n}/\nu, & d_{t_m,t_n} < \nu, \end{cases} \tag{46}$$

here $\gamma(t_m,t_n)$ is the correlation index of ILPHVG$_n(\rho)$ at time t_m and at time t_n and $\gamma(t_m,t_n)$ can be visualized using a recursive graph G, constructed using the formula

$$G(t_m,t_n) = \Theta\left(\nu - d_{t_m,t_n}\right), \tag{47}$$

where $\Theta(x)$ is the Heaviside function. We use this formula to plot the dependence between $ILPHVG_n(\rho,t_m)$ and $ILPHVG_n(\rho,t_n)$ in two-dimensional coordinates, in which both the abscissa and the ordinate are the time t. In the recursive graph, when the Euclidean distance between $ILPHVG_n(\rho,t_m)$ and $ILPHVG_n(\rho,t_n)$ is sufficiently close, i.e., when $G(t_m,t_n) = 1$, we plot a dot at (t_m,t_n) and (t_n,t_m). Note that at (t_m,t_m) and (t_n,t_n), i.e., the dots remain in the main diagonal, and we can use this result to characterize the global dynamic changes in correlation γ. Using Eq. (46), we can obtain the degree correlation index matrix $\{\gamma_d(i,t)\}$ and the clustering coefficient correlation index matrix $\{\gamma_c(i,t)\}$ with i and $t = 1,2,...,T'$.

Step 4. Measure the systematic risk. According to the information entropy, we develop a degree correlation index

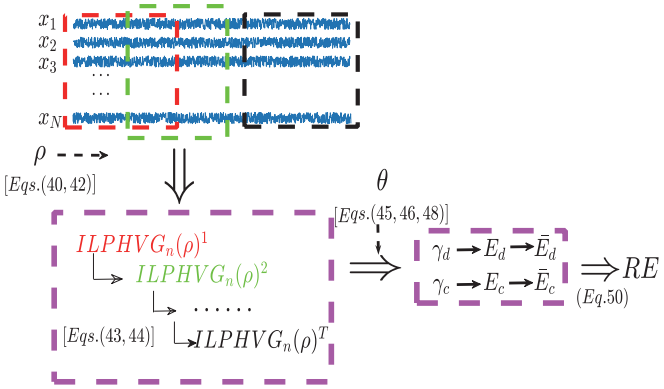

FIG. 11. Detailed procedure of the proposed method for systematic risk measuring.

entropy, denoted as S_d and the clustering coefficient correlation index entropy, denoted as S_c, which is calculated by

$$S_d(t) = -\sum_{i=1}^{T'} P_d(i,t)\log[P_d(i,t)], P_d(i,t) = \frac{\gamma_d(i,t)}{\sum_{i=1}^{T'}\sum_{t=1}^{T'}\gamma_d(i,t)}, \quad (48)$$

$$S_c(t) = -\sum_{i=1}^{T'} P_c(i,t)\log[P_c(i,t)], P_c(i,t) = \frac{\gamma_c(i,t)}{\sum_{i=1}^{T'}\sum_{t=1}^{T'}\gamma_c(i,t)}, \quad (49)$$

then the risk measurement formula R can be obtained,

$$R(t) = \omega_1 \bar{S}_d(t) + \omega_2 \bar{S}_c(t), \quad (50)$$

where ω_i is the weight, and $\bar{S}_d(t)$ and $\bar{S}_c(t)$ are the normalized vector of $S_d(t)$ and $S_c(t)$, respectively. The procedure of the proposed method for systematic risk measuring is illustrated in Fig. 11.

We choose the crude oil import values (unit: US Dollar thousand) of 38 crude-oil-import-dependent countries as the sample data, i.e., $N = 38$. The data cover the period from January 2005 to December 2014 and consist of 120 monthly observations, i.e., $T = 120$. All the data were obtained from the US Energy Information Administration. We use the Z-score standardizing processing method for data processing and the standardized data is obtained as shown in Fig. 12(a). From step 1, we set the length of sliding window $L = N = 38$ because this is the number of crude-oil-import-dependent countries. To ensure that there are enough sliding windows, we set the step length between the time windows equal to 1, i.e., $l = 1$. Therefore, we obtain $T' = (M - L)/l + 1 = 83$ small-scale time windows. We use Eqs. (40) and (42) to calculate the values of χ^2 and $\Delta(\rho)$ with ρ changing from 0 to 9. Figure 12(b) plots the values of χ^2 of the real data and the random data. Figure 12(c) shows how the values of $\Delta(\rho)$ changes with ρ. We find that when $\rho = 3$, the value of Δ reaches the maximum, thus we choose $\rho = 3$ to build ILPHVG$_n(\rho)$s. We set $n = 8$ and by using Eqs. (43)–(45), we perform 100 simulations of the random matrix to obtain

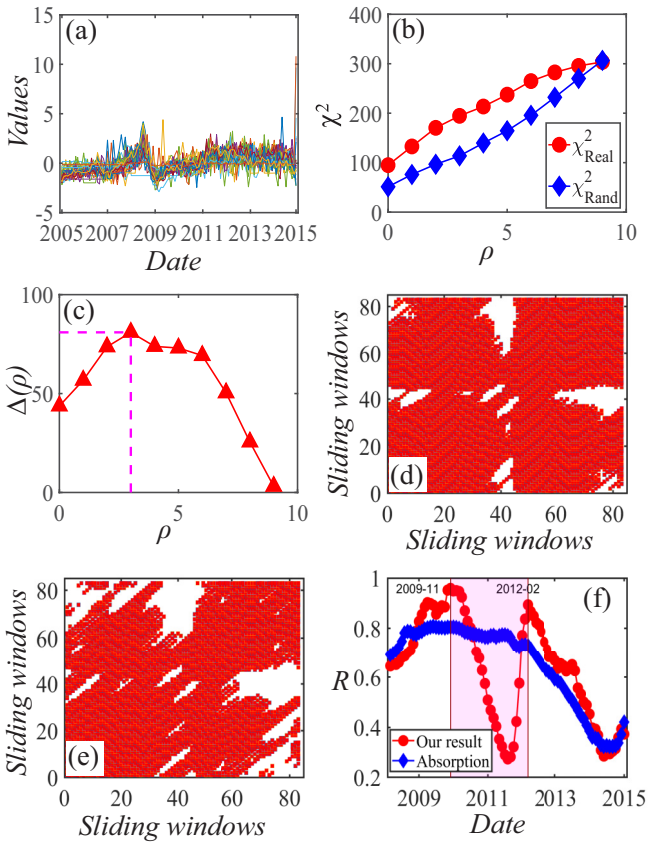

FIG. 12. (a) The selected sample of real data for crude oil import values. (b) χ^2 for the real data and for random data, respectively. (c) $\phi(\rho)$ dependence on ρ. (d) The recursive graph of degree correlation index matrix, (e) recursive graph of clustering coefficient correlation index matrix, (f) the evolution of the systematic risk.

9031 and 334 for the threshold values of degree and clustering coefficient, respectively. Then, using Eqs. (46) and (47), we obtain the degree correlation index matrix $\{\gamma_d(i,j)\}$ and the clustering coefficient correlation index matrix $\{\gamma_c(i,j)\}$ of the system for crude-oil-import-dependent countries. The results are shown in Figs. 12(d) and 12(e) where we can clear see that the crude-oil-import-dependent countries system has both short-range and long-range correlations. Figure 12(f) plots the evolution of the systematic risk, where the red cycle line is our result, and the blue diamond line is the result using the absorption rate in literature which is also a measurement of systematic risk [44]. Figure 12(f) indicates that the period of the evolution of the risk in crude oil supply was divided into three different periods. Before November 2009, the risk in crude oil supply showed a upward trend due to the financial crisis. Then the risk showed a trend of shock between December 2009 and February 2012, and after February 2012 the risk shocked in a downward trend, and down to the minimum on June 2014. Our method can better reflect the evolutionary process of the risk than the absorption rate; this is because this quantity is just the sum of eigenvalues. The idea of absorption rate is to measure systemic risk using the volatility of eigenvalues but this method ignores the influence of other effects on the systematic risk. Our proposed calculation formula [Eqs. (48)–(50)] can be used to solve the problem of quantitative measures of the risk

because it comprehensively considers effects of several factors on system risk. Integrating the volatility and the real market information, our calculation formula decrypts system risk into a more reasonable final result.

V. DISCUSSIONS

We have introduced a directed-limited penetrable horizontal visibility graph DLPHVG(ρ) and an image-limited penetrable horizontal visibility graph [ILPHVG$_n(\rho)$], both inspired by the limited penetrable horizontal visibility graph LPHVG(ρ) [34]. These two algorithms are expansions of the limited penetrable horizontal visibility algorithm. We first derive theoretical results on the topological properties of LPHVG(ρ), including degree distribution $P(k)$, mean degree $\langle k\rangle$, the relation between the datum height x and the mean degree $\langle k(x)\rangle$ of the nodes associated to data with a height equal to x, the normalized mean distance $\langle d\rangle$, the local clustering coefficient distribution $P(C_{\min})$ and $P(C_{\max})$, and the probability of long distance visibility $P_\rho(n)$. We then deduce the in and out degree distributions $P_{\text{in}}(k)$ and $P_{\text{out}}(k)$ of DLPHVG(ρ), and the degree distribution of ILPHVG$_n(\rho)$. We perform several numerical simulations to check the accuracy of our analytical results. Furthermore, we propose a method for deriving degree distributions of LPHVG(ρ), DLPHVG(ρ), and ILPHVG$_n(\rho)$ by using an iterative construction process of LPHVG(ρ), DLPHVG(ρ), and ILPHVG$_n(\rho)$. In particular, we take ILPHVG$_n(\rho)$ for example and give a detailed proof process. The proposed iterative construction approach for deriving degree distributions is simple to calculate and can be applied for more complicated time series, such as Logistic maps and fractional Brownian motions.

We then present applications of the directed-limited penetrable horizontal visibility graph and the image-limited penetrable horizontal visibility graph, including measuring the irreversibility of a real-value time series and discriminating between noise and chaos. Empirical results consistent with the results in references [33,39]. To further demonstrate the practicality of our method, we propose a method to measure the systematic risk using ILPHVG$_n(\rho)$, and empirical results testify the efficiency of our methods.

Our theoretical results on topological properties are an extension of previous findings [22,32–34]. In the structure of the limited penetrable horizontal visibility graph family, the limited penetrable parameter ρ is important and affects the structure of the associated graphs. Using certain ρ values, the exact results of the associated graphs reveals the essential characteristics of the system, e.g., when $\rho = 0$ and $\rho = 1$, using the degree distribution of ILPHVG$_8(\rho)$, we can distinguish between uncorrelated and weakly coupled systems. But when $\rho = 2$, the distinction is no longer clear [see Fig. 10(c)]. Although we have given a method to determine ρ in this paper, how to use real data to select an optimal limited penetrable parameter ρ is still a interesting problem. As we know, extracting the underlying dynamic processes is an important topic in the analysis of time-series of complex dynamical systems. Recently, Scholz et al. [41] proposed a direct method to obtain the deterministic and stochastic contribution of the sum of two independent stochastic processes. Rinn *et al.* [42] presented an R package for stochastic data analysis that is able to extract the stochastic evolution equations of physical properties from sets of their measurements: how to use the framework of limited penetrable horizontal visibility graphs to distinguish between additive and multiplicative stochastic contributions in superposed time series; how to use this framework to uncover dynamical features of its (chaotic or not) deterministic part. We will introduce the concept of subgraphs of limited penetrable horizontal visibility graphs and try to address these questions by using the distribution of subgraphs in our further research.

ACKNOWLEDGMENTS

The Research was supported by the following foundations: The National Natural Science Foundation of China (Grants No. 71503132, No. 71690242, No. 91546118, No. 11731014, No. 71403105, and No. 61403171); Qing Lan Project of Jiangsu Province (Grant No. SJ201715), University Natural Science Foundation of Jiangsu Province (Grant No. 14KJA110001); Jiangsu Center for Collaborative Innovation in Geographical Information Resource Development and Application, CNPq, CAPES, FACEPE and UPE (Grants No. APQ-0565-1.05/14, and No. PFA2016, No. PIAEXT2016); the program of China Scholarship Council (Grant No. 201606770023). The Boston University Center for Polymer Studies is supported by NSF Grants No. PHY-1505000, No. CMMI-1125290, and No. CHE-1213217; by DTRA Grant No. HDTRA1-14-1-0017; and by DOE Grant No. DE-AC07-05ld14517.

[1] Z. Gao, M. Small, and J. Kurths, Europhys. Lett. **116**, 50001 (2017).
[2] J. Zhang and M. Small, Phys. Rev. Lett. **96**, 238701 (2006).
[3] L. Lacasa, B. Luque, F. Ballesteros, J. Luque, and J. C. Nuño, Proc. Natl. Acad. Sci. USA **105**, 4972 (2008).
[4] N. Marwan, J. F. Donges, Y. Zou, R. V. Donner, and J. Kurths, Phys. Lett. A **373**, 4246 (2009).
[5] A. H. Shirazi, G. R. Jafari, J. Davoudi, J. Peinke, M. R. R. Tabar, and M. Sahimi, J. Stat. Mech. Theory Exp. (2009) P07046.
[6] Y. Zhao, T. Weng, and S. Ye, Phys. Rev. E **90**, 012804 (2014).
[7] J. F. Donges, Y. Zou, N. Marwan, and J. Kurths, Europhys. Lett. **87**, 48007 (2009).
[8] V. Stolbova, P. Martin, B. Bookhagen, N. Marwan, and J. Kurths, Nonlin. Process. Geophys. **21**, 901 (2014).
[9] M. Wang and L. Tian, Physica A (Amsterdam) **461**, 456 (2016).
[10] C. Zhou, L. Ding, M. J. Skibniewski, H. Luo, and S. Jiang, Saf. Sci. **98**, 145 (2017).
[11] P. Oświęcimka, L. Livi, and S. Drożdż, Phys. Rev. E **94**, 042307 (2016).
[12] Z. Gao, S. Li, W. D. Dang, Y. X. Yang, Y. Do, and C. Grebogi, Int. J. Bifurcat. Chaos **27**, 1750123 (2017).
[13] M. Wang, Y. Chen, L. Tian, S. Jiang, Z. Tian, and R. Du, Appl. Energy **175**, 109 (2016).
[14] M. Wang, L. Tian, and R. Du, Appl. Energy **180**, 779 (2016).

[15] M. Wang, L. Tian, H. Xu, W. Li, R. Du, G. Dong *et al.*, Physica A (Amsterdam) **473**, 188 (2017).
[16] H. Chen, L. Tian, M. Wang, and Z. Zhen, Sustainability **9**, 574 (2017).
[17] R. Du, Y. Wang, G. Dong, L. Tian, Y. Liu, M. Wang *et al.*, Appl. Energy **196**, 142 (2017).
[18] R. Du, G. Dong, L. Tian, M. Wang, G. Fang, and S. Shao, PloS one **11**, e0162362 (2016).
[19] J. Xiao, M. Wang, L. Tian, and Z. Zhen, Physica A (Amsterdam) **490**, 664 (2018).
[20] Y. Li, D. Yang, and X. J. Li, Math. Finance **7**, 734 (2017).
[21] I. V. Bezsudnov and A. A. Snarskii, Physica A (Amsterdam) **414**, 53 (2014).
[22] B. Luque, L. Lacasa, F. Ballesteros, and J. Luque, Phys. Rev. E **80**, 046103 (2009).
[23] L. Lacasa, B. Luque, J. Luque, and J. C. Nuño, Europhys. Lett. **86**, 30001 (2009).
[24] R. Ray, M. H. Khondekar, K. Ghosh, and A. K. Bhattacharjee, Theor. Appl. Climatol. **124**, 119 (2016).
[25] G. Gutin, T. Mansour, and S. Severini, Physica A (Amsterdam) **390**, 2421 (2011).
[26] T.-T. Zhou, N.-D. Jin, Z.-K. Gao, and Y.-B. Luo, Acta. Phys. Sin. **61**, 030506 (2012).
[27] Z.-K. Gao, L.-D. Hu, T.-T. Zhou, and N.-D. Jin, Acta Phys. Sin. **62**, 110507 (2013).
[28] Z. Gao, Q. Cai, Y. Yang, W. Dang, and S. Zhang, Sci. Rep. **6**, 1 (2016).
[29] J. Wang, C. Yang, R. Wang, H. Yu, Y. Cao, and J. Liu, Physica A (Amsterdam) **460**, 174 (2016).
[30] R. X. Wang, J. M. Gao, Z. Y. Gao, X. Gao, and H. Q. Jiang, Sci. China Technol. Sc. **59**, 604 (2016).
[31] B. Luque, L. Lacasa, F. J. Ballesteros, and A. Robledo, Chaos **22**, 013109 (2012).
[32] L. Lacasa, Nonlinearity **27**, 2063 (2014).
[33] L. Lacasa and J. Iacovacci, Phys. Rev. E **96**, 012318 (2017).
[34] M. Wang, A. L. M. Vilela, R. Du, L. Zhao, G. Dong, L. Tian, and H. E. Stanley, Sci. Rep. **8**, 5130 (2018).
[35] R. Kawai, J. M. R. Parrondo, and C. Van den Broeck, Phys. Rev. Lett. **98**, 080602 (2007).
[36] M. Costa, A. L. Goldberger, and C. K. Peng, Phys. Rev. Lett. **95**, 198102 (2005).
[37] D. Andrieux, P. Gaspard, S. Ciliberto, N. Garnier, S. Joubaud, and A. Petrosyan, Phys. Rev. Lett. **98**, 150601 (2007).
[38] M. B. Kennel, Phys. Rev. E **69**, 056208 (2004).
[39] L. Lacasa, È. Nuñez, A. Roldán, J. M. R. Parrondo, and B. Luque, Eur. Phys. J. B **85**, 217 (2012).
[40] O. A. Rosso, H. A. Larrondo, M. T. Martin, A. Plastino, and M. A. Fuentes, Phys. Rev. Lett. **99**, 154102 (2007).
[41] T. Scholz, F. Raischel, V. V. Lopes, B. Lehle, M. Wächter, J. Peinke, and P. G. Lind, Phys. Lett. A **381**, 194 (2017).
[42] P. Rinn, P. G. Lind, M. Wächter, and J. Peinke, J. Open Res. Softw. **4**, e34 (2016).
[43] P. Smaga, Systemic Risk Centre Special Paper **5**, 1 (2014).
[44] H. Meng, W. J. Xie, Z. Q. Jiang, B. Podobnik, W. X. Zhou, and H. E. Stanley, Sci. Rep. **4**, 3655 (2014).
[45] C. T. Brownlees and R. Engle, working paper, New York University (2012).
[46] A. Murks and M. Perc, Adv. Complex Syst. **14**, 307 (2011).
[47] B. Podobnik, D. Horvatic, T. Lipic, M. Perc, J. M. Buldú, and H. E. Stanley, J. Roy. Soc. Interface **12**, 20150770 (2015).
[48] X. Zhang, B. Podobnik, D. Y. Kenett, and H. E. Stanley, Physica A (Amsterdam) **415**, 43 (2014).
[49] X. Zhang, L. Feng, Y. Berman, N. Hu, and H. E. Stanley, Europhys. Lett. **116**, 18001 (2016).
[50] G. Girardi and A. T. Ergün, J. Bank. Finance **37**, 3169 (2013).